Adsorption 11: 113–122, 2005

A New Numerical Method for Accurate Simulation of Fast Cyclic Adsorption Processes

HYUNGWOONG AHN AND STEFANO BRANDANI*
Department of Chemical Engineering, University College London, Torrington Place, London WC1E 7JE, UK
s.brandani@ucl.ac.uk

Received July 21, 2004; Revised May 10, 2005; Accepted August 2, 2005

Abstract. In the simulation of fast cyclic adsorption processes, to apply the Fickian diffusion model it is necessary to include an increasing number of numerical discretization points as the cycle time is reduced in comparison to the characteristic diffusional time constant.

We propose a new numerical method based on the definition of two distinct regions within an adsorbent particle: an outer layer where the concentration varies significantly with large internal gradients leading to enhanced mass fluxes, and an internal region where the concentration profile is virtually flat. The proposed method leads to the automated generation of a numerical grid that has a constant number of elements independent of the process cycle time. The procedure is demonstrated on a model for the simulation of a heatless dryer pressure swing adsorption process.

Keywords: diffusion model, adsorption, numerical simulation, cyclic adsorption processes

Introduction

When the diffusional time constant R^2/D is large compared to the cycle time, the internal concentration profiles vary rapidly within a short section close to the solid's surface where the external concentration is fluctuating. In the simulation of fast cyclic adsorption processes, to apply the Fickian diffusion model it is necessary to include an increasing number of numerical discretization points as the cycle time is reduced in comparison to the characteristic diffusional time constant. A numerical approach which uses a discretization scheme based on equally spaced elements has to be tested iteratively in order to establish the minimum number of intervals needed to avoid numerical dispersion of the adsorbent concentration profile. The problem is compounded if one includes an adsorption simulation code within an optimization package aimed at determining the optimal cycle time. In this case the actual computational time required for an individual process simulation becomes important.

In order to simplify the model and shorten the simulation time, it is also possible to apply a lumped model, i.e. the Linear Driving Force (LDF) approximation, but this requires a cycle time dependent correction (Nakao and Suzuki, 1983). The LDF equivalence (Nakao and Suzuki, 1983) predicts an increase in the mass transfer rates that is consistent with the increased internal concentration gradients, but it can only match the amplitude ratios of the concentration and does not yield the correct phase lag. In order to obtain the correct cyclic steady state (CSS) concentration profiles, we suggested recently that the solid volume should be corrected (Rouse and Brandani, 2001) to take into account only the active section of the adsorbent particle. Even though the new LDF approximation was in a excellent agreement with the diffusion model at CSS, it does not describe correctly the transient behaviour since the system capacity is reduced in order to take into account the fact that at CSS the internal part of the

*To whom all correspondence should be addressed.

solid adsorbent is unaffected by the varying external concentration.

To describe the full transient behaviour it is therefore necessary to use the diffusion model. Based on the observation that the LDF approximation is still valid when one describes the adsorbent as two separate regions, it is possible to apply a similar approach to the numerical solution of the diffusion equation for fast cyclic processes. The internal concentration profile for fast cyclic adsorption processes is therefore characterised by two distinct regions: an outer layer where the concentration varies significantly with large internal gradients leading to enhanced mass fluxes, and an internal region where the concentration profile is virtually flat. The aim of this contribution is to develop a predictive method to assign a numerical grid for the solution of the diffusion equation for fast cyclic adsorption processes that is scaled so that the number of collocation intervals is independent of the cycle time.

Determination of the Location of the Internal Solid Boundary

We will consider the case of a spherical adsorbent particle and observe the main features of the solution of the diffusion equation at CSS.

The mass balance in the particle is

$$\frac{\partial q}{\partial t} = D\left(\frac{\partial^2 q}{\partial r^2} + \frac{2}{r}\frac{\partial q}{\partial r}\right) \tag{1}$$

with the associated boundary conditions

$$\left.\frac{\partial q}{\partial r}\right|_{r=0} = 0 \tag{2}$$

$$q|_{r=R} = Kc \tag{3}$$

The second boundary condition, Eq. (3), is written assuming equilibrium at the surface, which is taken to be linear. The solution would be the same if we imposed simply that the solid concentration at the surface is a cyclic function of time. The main assumption is in fact that the diffusivity is independent of concentration in Eq. (1).

Defining the dimensionless variables and parameters using the half cycle time, t_C,

$$\xi = \frac{r}{R_p} \quad \tau = \frac{t}{t_c} \quad Q = \frac{q}{q_0} \quad C = \frac{c}{c_0} \quad a = \frac{Dt_C}{R_p^2} \tag{4}$$

and assuming an initially empty solid, the analytical solution to Eq. (1) can be found in the Laplace domain to be

$$\tilde{Q} = \frac{\sinh\left(\sqrt{\frac{s}{a}}\xi\right)}{\sinh\left(\sqrt{\frac{s}{a}}\right).\xi}\tilde{C} \tag{5}$$

where s is the Laplace domain variable. The term that multiplies the external concentration, on the RHS of Eq. (5), is clearly the transfer function, G, of the process and from process control theory (Stephanopoulos, 1983) it is possible to find the CSS solution. Substituting $s = i\pi$ in the transfer function (Rouse and Brandani, 2001), the modulus will yield the amplitude ratio or attenuation and the argument will yield the phase lag.

If the following sinusoidal function is applied to the system as a disturbance

$$C = \frac{1}{2}\left[\sin(\pi\tau) + 1\right] \tag{6}$$

the internal concentration will be given by

$$Q = \frac{1}{2}\left[|G| \cdot \sin(\pi\tau + \arg(G)) + 1\right] \tag{7}$$

To study how the solid concentration profile varies it is also useful to consider the first and second order derivatives, which give an indication of how rapidly the concentration varies. In this case

$$\frac{\partial \tilde{Q}}{\partial \xi} = \frac{\xi\sqrt{\frac{s}{a}}\cosh\left(\sqrt{\frac{s}{a}}\cdot\xi\right) - \sinh\left(\sqrt{\frac{s}{a}}\cdot\xi\right)}{\xi^2\sinh\left(\sqrt{\frac{s}{a}}\right)}\tilde{C} \tag{8}$$

$$\frac{\partial^2 \tilde{Q}}{\partial \xi^2} = \frac{\frac{s}{a}\xi^2\sinh\left(\sqrt{\frac{s}{a}}\cdot\xi\right) - 2\xi\sqrt{\frac{s}{a}}\cosh\left(\sqrt{\frac{s}{a}}\cdot\xi\right) + 2\sinh\left(\sqrt{\frac{s}{a}}\cdot\xi\right)}{\xi^3\sinh\left(\sqrt{\frac{s}{a}}\right)}\tilde{C} \tag{9}$$

And the time domain solutions at CSS can be calculated from the corresponding transfer functions G_{d1} and G_{d2}.

$$\frac{\partial Q}{\partial \xi} = \frac{1}{2}|G_{d1}|.\sin[\pi\tau + \arg(G_{d1})] \tag{10}$$

$$\frac{\partial^2 Q}{\partial \xi^2} = \frac{1}{2}|G_{d2}|.\sin[\pi\tau + \arg(G_{d2})] \tag{11}$$

Figure 1 shows the concentration profiles at various intermediate times for different cycle times. Qualitatively the profiles are similar and we can clearly see the occurrence of two distinct regions. To define unambiguously the interface between the two regions is

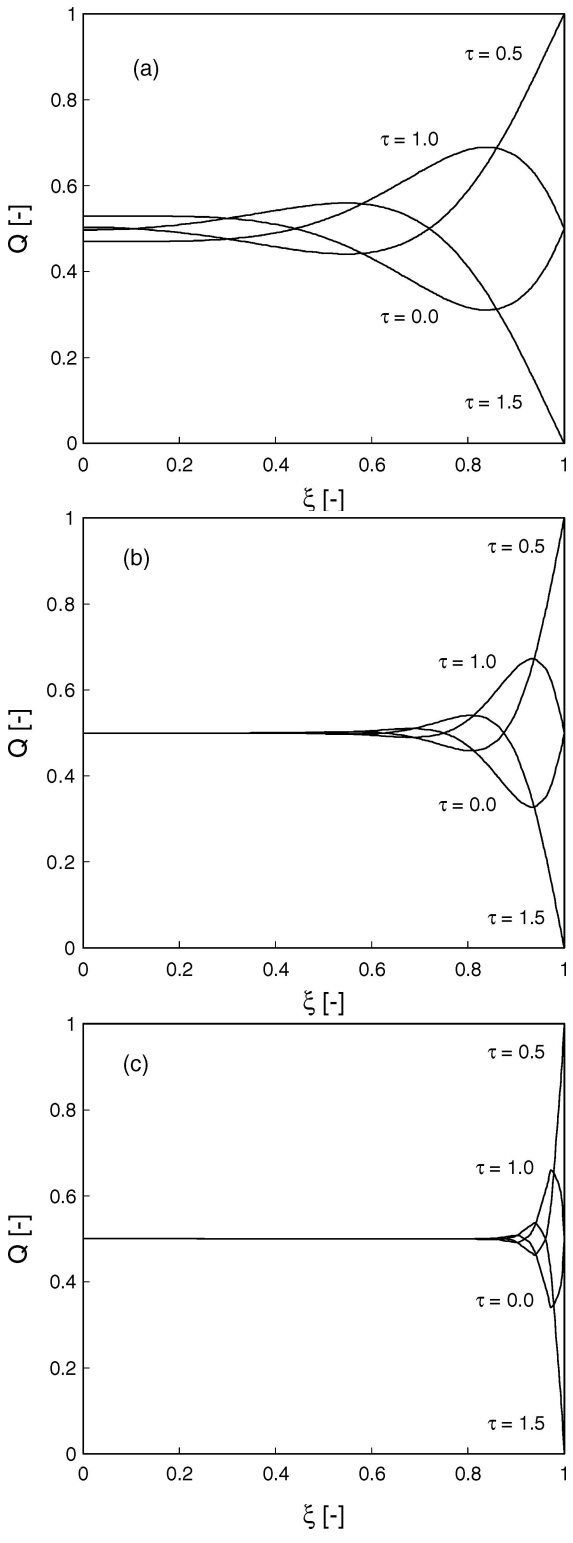

Figure 1. Concentration profiles for different half cycle times: (a) $a = 0.05$, (b) $a = 0.01$ and (c) $a = 0.001$.

useful to observe that the profiles resemble waves that propagate towards the centre of the adsorbent with large damping. The most important variable is the concentration gradient, and we choose as our reference the point where

$$\left|\frac{\partial Q}{\partial \xi}\right| = 0.05 \tag{12}$$

Note that there will be always a value of ξ that will satisfy Eq. (12) unless the external perturbation is so slow that the system operates under near equilibrium conditions.

Figure 2(a) shows the variation of the concentration in particle along the radial position at $\tau = 0$ for $a = 0.01$ and Fig. 2(b) shows the corresponding first and second order derivatives. As can be seen from Fig. 2(b) there are multiple solutions to Eq. (12) and these will vary with time. In this case we can identify up to five roots, but we are only interested in the minimum value of ξ that satisfies Eq. (12) at any time. It is not simple to find directly the inner root, since the first derivative fluctuates in this region. To find the solution in an automated way we observe that the gradient near the surface is monotonic for $\tau = 0$. Starting at $\xi = 1$ we will find always the first outer root for the positive gradient with any algorithm. If we do this for $\tau = 0$ and then choose a sufficiently small $\Delta\tau$, we can use the previous root to initiate the search and find the next solution, which will be moving towards the centre of the solid. By repeating the procedure we can easily generate a map of the solution for all $0 \leq \tau \leq 2$, which is shown in Fig. 3 for two representative cases. For $a > 0.025$ a curve obtained from this procedure has a minimum and only extends to a value of $\tau < 2$. For $a < 0.025$ the mapped solution is monotonically decreasing as we move from the outer solution to the inner one with time. This procedure guarantees convergence and it is not necessary to repeat it for the negative value of the gradient due to symmetry, as shown in Fig. 4. Table 1 reports the numerical values of the boundary location for different dimensionless cycle times.

Figure 5 shows the values of the interface for different cycle times. A simple log–log correlation represents all the values and can be used as a quick estimate. If one considers that for very fast cycles the penetration length scales with $\sqrt{a}$ (Crank, 1975), we can see that the empirical exponent 0.46 is close to the theoretical 0.5 value.

Having assigned a very low value for the maximum gradient in the inner domain, only one grid point will

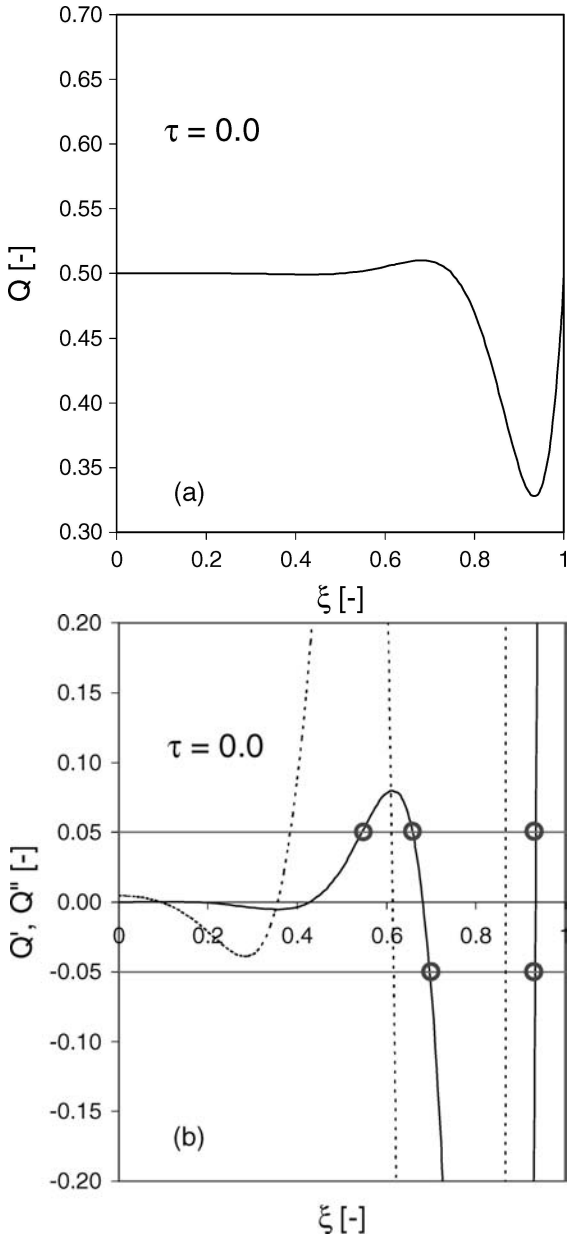

Figure 2. (a) Concentration profile (a) and (b) first and second derivatives (dotted line) along the radial position at $\tau = 0$ for $a = 0.01$.

be allocated to describe accurately the concentration profile in this region. The outer domain requires a fixed number of grid points which will depend on the numerical scheme used. In gPROMS (PSE, 1999), we found that using orthogonal collocation on finite elements (OCFEM), four collocation intervals are required to capture all the features of the internal concentration

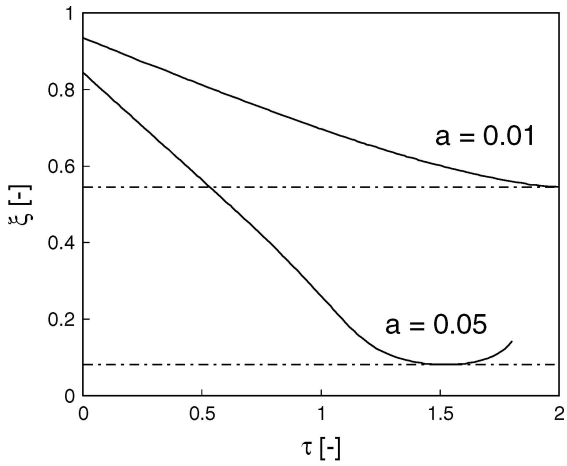

Figure 3. Roots found starting at $\xi = 1$ for $\tau = 0$.

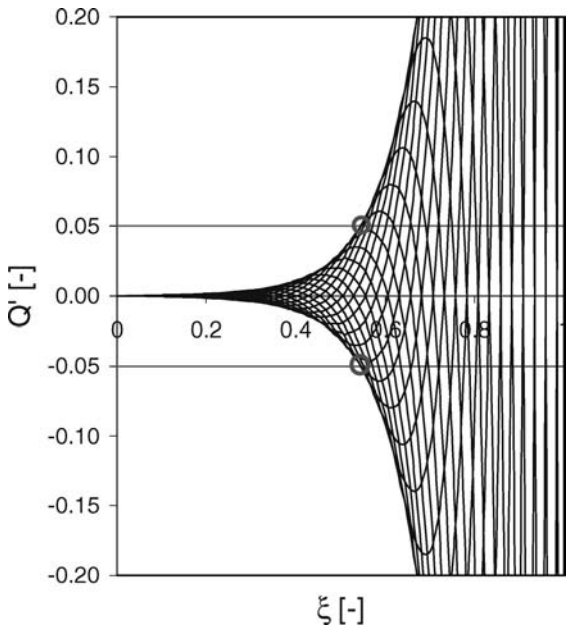

Figure 4. Internal concentration gradients as a function of time for $a = 0.01$. Curves shown are at 0.1 reduced time intervals between 0 and 2. Also shown is the minimum ξ that satisfies Eq. (12) found from the algorithm described in the text.

profile. To close the problem the following boundary conditions at the inner/outer domain interface, which guarantee continuity and mass conservation, are applied:

$$Q_i|_{\xi=R_b} = Q_o|_{\xi=R_b} \tag{13}$$

$$\left.\frac{\partial Q_i}{\partial \xi}\right|_{\xi=R_b} = \left.\frac{\partial Q_o}{\partial \xi}\right|_{\xi=R_b} \tag{14}$$

Table 1. Variation of the boundary location with dimensionless cycle.

a	R_b
0.05	0.082
0.01	0.545
0.005	0.671
0.001	0.843
0.0005	0.886
0.0001	0.947
0.00005	0.962

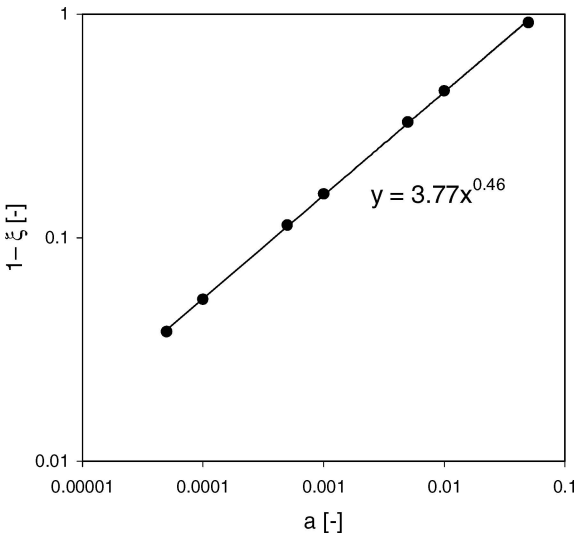

Figure 5. Correlation of the boundary location.

Note that being able to predict the position of the interface, allows also the simple estimation of the minimum number of equally spaced intervals needed to reproduce accurately the internal concentration profile. This is achieved by ensuring that one has at least the same number of grid intervals in the outer region as in the case of the two domain grid.

CSTR Simulations

The validity of the two-domain approach was evaluated initially through the simulation of a CSTR model with a sinusoidal input function using gPROMS (PSE, 1999).

The mass balance in the gas phase is

$$V_s \frac{\partial \bar{q}}{\partial t} + V_f \frac{\partial c}{\partial t} + F(c - c_{\text{in}}) = 0 \qquad (15)$$

The mass balance in the adsorbed phase is given by Eq. (1) and the average concentration in the adsorbed phase can be replaced by

$$\frac{\partial \bar{q}}{\partial t} = 3 \frac{D}{R_p} \cdot \frac{\partial q}{\partial r}\bigg|_{r=1} \qquad (16)$$

The following dimensionless parameters are defined in addition to Eq. (4).

$$\gamma = \frac{V_f}{3 V_s K} L = \frac{1}{3} \frac{F}{K V_s} \frac{R_p^2}{D} \qquad (17)$$

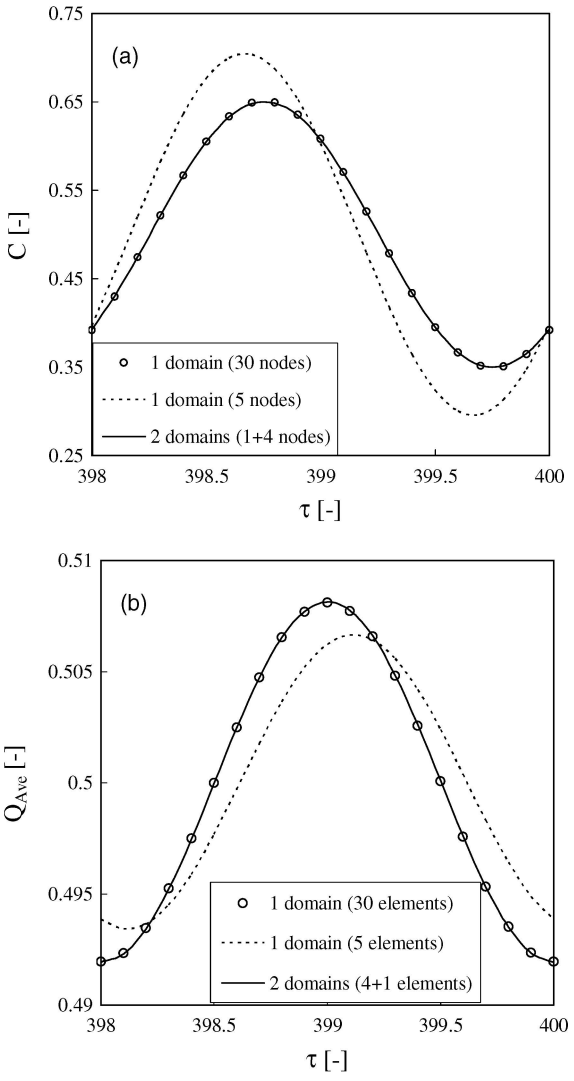

Figure 6. CSTR simulations for $\gamma = 0.01$, $L = 30$ and $a = 0.001$. (a) gas phase concentration; (b) average solid phase concentration.

With the dimensionless variables and parameters, Eqs. (15–16) become

$$\gamma \frac{\partial C}{\partial \tau} = -a \frac{\partial Q}{\partial \xi}\bigg|_{\xi=1} - a \cdot L(C - C_{\text{in}}) \quad (18)$$

$$\frac{\partial \bar{Q}}{\partial \tau} = 3a \cdot \frac{\partial Q}{\partial \xi}\bigg|_{\xi=1} \quad (19)$$

The simulations of this simple model allow rapid testing of the new approach and more importantly we can gain insight into the effect of using too few numerical grid intervals. Figure 6 shows the gas phase and solid phase average concentration at CSS (after 200 cycles) for $a = 0.001$; $L = 30$; $\gamma = 0.01$. The L and γ values are typical of gas systems encountered in practice in a ZLC system (Brandani and Ruthven, 1996). In the case of $a = 0.001$, 30 nodes for the radial direction should be used in the one-domain grid in order to simulate the dynamics accurately. Figure 6 shows that the two-domain approach yields exactly the same results. Furthermore, we can see that the one-domain with five elements yields gas phase concentrations that are incorrect both in terms of amplitudes and phase lags. Note that the solution for five equally spaced intervals would be found to be incorrect only by repeating the calculation and increasing the number of grid elements, i.e. by trial and error.

Table 2 reports the comparison of the execution time and problem size for the two-domain approach and the equally spaced one-domain grid with equal accuracy. The results show that the two-domain method is essentially independent of cycle time and is only slightly more cumbersome for slow cycles. Note that for the one-domain solution the number of grid elements increases exponentially and that the simulation times are still reasonable due to the efficiency of gPROMS that automatically makes use of sparse matrices algorithms.

Table 2. Comparison of the simulation time for 200 cycles for the CSTR model ($\gamma = 0.01$; $L = 30$).

	One-domain		Two-domain	
A	Simulation time (sec)	Required number of nodes	Simulation time (sec)	Required number of nodes
0.05	5.050	5	6.430	5 nodes (1 node for inner domain + 4 nodes for outer domain)
0.01	5.930	10	6.210	
0.005	7.970	15	7.360	
0.001	10.490	30	7.150	
0.0005	12.580	40	7.190	
0.0001	19.230	80	7.420	
0.00005	20.820	110	7.140	

Simulation of a Heatless Drier PSA Process

As a test system to compare the efficiency of the new numerical method on a sufficiently large problem, we consider the heatless drier model of Raghavan et al. (1986). The emphasis here is not on modifying or improving the mathematical model but on comparing simulation times for both dynamic and direct CSS calculations between an equally spaced dense grid (one-domain method) and the proposed two-domain method with $4 + 1$ elements.

The process is a standard 4 step PSA system and the model of Raghavan et al. (1986) is based on the following general assumptions:

(1) The system is isothermal.
(2) The ideal gas law is applied.
(3) The effect of pressure drop along the bed is negligible.
(4) The flow pattern is described by an axial dispersed plug flow.
(5) Fluid velocity is not affected by the effect of adsorption because sorbate is regarded as a trace component.

We assume linear equilibrium and the parameters used in the simulation are listed in Table 3 with the timing of the four steps taken from Raghavan et al. (1986). The model equations are reported in the appendix.

We simulated the PSA process for $a = 0.005$, which corresponds to a half-cycle time of approximately 3 min, for 300 cycles which are required to reach CSS from an initially empty bed. In the simulation performed on gPROMS (PSE, 1999), the total number of elements required inside the solid particles for the one-domain method is 13. The axial direction is discretised using 10 elements. The PSA model was also coded for the direct solution of the cyclic steady state problem (Nilchan and Pantelides, 1998) using 20 collocation elements to discretise the cycle time.

Figure 7 shows the variation of the mole fraction at the product end of bed 1 during the last two cycles of the dynamic simulations, which coincide with the result

Table 3. Summary of parameters used in the simulation of heatless dryer PSA process (Raghavan et al., 1986).

Adsorption bed	
L (m)	1
ε (−)	0.4
ε_p (−)	0.34
K (−)	18168
D_p/R_p^2 (s^{-1})	0.168
Adsorption conditions	
y_f (−)	0.003926
P_H (atm)	5
u_H (m/s)	0.5
Purge conditions	
P_L (atm)	1
u_L (m/s)	1
Configuration of step timings in a cycle	
Adsorption and purge step time, τ_{AD} and τ_{PG} (−)	0.75
Pressurization and blowdown step time, τ_{PR} or τ_{BD} (−)	0.25

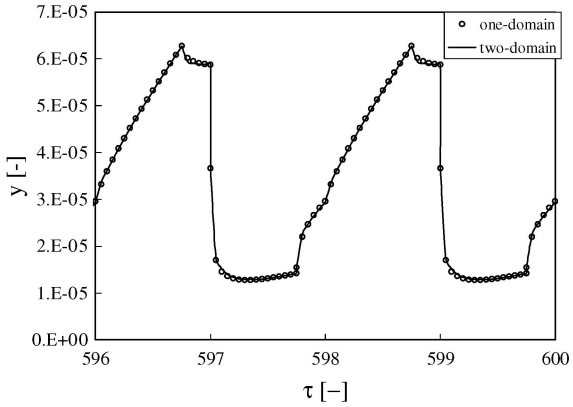

Figure 7. Simulation of the heatless drier PSA model for $a = 0.005$ at cyclic steady state.

obtained from the direct cyclic steady state simulation. Figure 8 represents the ratio of the concentration at the end of adsorption step to the feed concentration as a function of time showing convergence to cyclic steady state at 300 cycles. From these figures it is evident that the two-domain approach reproduces exactly the full simulations confirming the validity of the method for both cyclic steady state simulations and the approach to CSS.

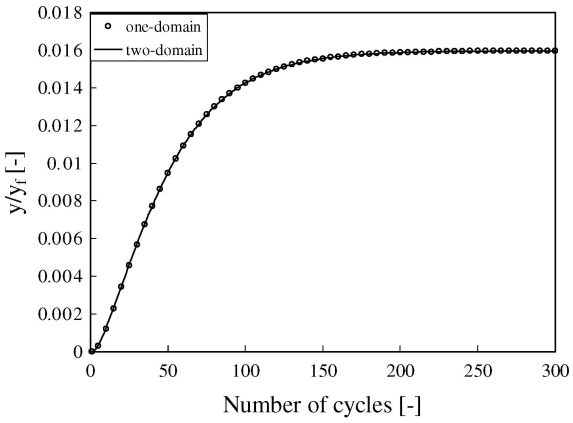

Figure 8. Outlet concentration at the end of the adsorption step as a function of the cycle number.

The two-domain approach reduces the size of the numerical problem by a factor 5/13, which roughly corresponds to the improvement in simulation times. For the dynamic simulations of 300 cycles, the simulation time was reduced from 8044 to 2835 s. For the direct cyclic steady state calculations the simulation time was reduced from 2939 to 532 s on a Pentium 4 PC. The fact that the reduction in simulation time is nearly proportional to the reduction in the number of equations to solve is an indication of the fact that gPROMS utilises highly efficient numerical algorithms for sparse matrices.

Conclusions

We have shown that the concentration profile inside a solid particle can be represented by two distinct regions and the location of the boundary between the inner and outer domains has been defined and correlated. To be able to predict the location of the boundary allows the simple estimation of the density of the numerical grid required to reproduce accurately the solution to the diffusion equation.

We have shown that a new numerical method can be used to fix the number of grid elements required for the representation of the solution to the diffusion equation in fast cyclic adsorption processes, with an approach that results in simulation times which are independent of cycle time.

The CSTR simulations have shown that too few equally spaced grid elements result in calculated gas phase concentrations with deviations in both amplitude

ratios and phase lags when compared with the correct numerical solution.

The new numerical method has been applied to the simulation of a heatless drier PSA process, showing that, for a highly efficient simulator such as gPROMS, the improvement in simulation times is roughly proportional to the reduction in the size of the grid.

Appendix

The mass balance in gas phase is

$$\frac{\partial c}{\partial t} = D_L \frac{\partial^2 c}{\partial z^2} - \frac{\partial (v \cdot c)}{\partial z} - \frac{1-\varepsilon}{\varepsilon}\frac{\partial q}{\partial t} \tag{A1}$$

With the linear isotherm the mass balance in adsorbed phase is

$$\frac{\partial c_p}{\partial t} = D_e\left(\frac{\partial^2 c_p}{\partial r^2} + \frac{2}{r}\frac{\partial c_p}{\partial r}\right) \tag{A2}$$

$$D_e = \frac{\varepsilon D_p}{\varepsilon + (1-\varepsilon)K} \tag{A3}$$

The dimensionless variables are

$$\tau = \frac{t}{t_C} \quad \zeta = \frac{z}{L} \quad \xi = \frac{r}{R_p} \quad y = \frac{c}{c_t} \quad y_p = \frac{c_p}{c_t}$$
$$V = \frac{v}{v_H} \quad \vec{P} = \frac{P}{P_H} \quad V_r = \frac{V_L}{V_H} \quad P_r = \frac{P_L}{P_H} \tag{A4}$$

The dimensionless parameters are

$$Pe = \frac{v_H L}{D_L} \qquad W = \frac{v_H R_p^2}{D_e L}$$
$$k = \frac{1-\varepsilon}{\varepsilon}K \qquad a = \frac{t_C D_e}{R_p^2} \tag{A5}$$

With the assumption of no pressure drop, the mass balance in gas phase is expressed in the following dimensionless form.

$$\frac{\partial y}{\partial \tau} = -\frac{y}{\bar{P}} \cdot \frac{\partial \bar{P}}{\partial t} + \frac{W \cdot a}{Pe}\frac{\partial^2 y}{\partial \zeta^2} - W \cdot a \frac{\partial (V \cdot y)}{\partial \zeta} - 3a \cdot k \cdot \left.\frac{\partial y_p}{\partial \xi}\right|_{\xi=1} \tag{A6}$$

The dimensionless mass balance in the adsorbed phase is

$$\frac{\partial y_p}{\partial \tau} = a\left(\frac{\partial^2 y_p}{\partial \xi^2} + \frac{2}{\xi}\frac{\partial y_p}{\partial \xi}\right) \tag{A7}$$

The associated boundary conditions at both ends of the column are as follows.

Step 1: adsorption step in bed 1 and purge step in bed 2

$$\left.\frac{\partial y_1}{\partial \zeta_1}\right|_{\zeta_1=0} = -Pe(y_f - y_1|_{\zeta=0}) \quad \left.\frac{\partial y_1}{\partial \zeta_1}\right|_{\zeta_1=1} = 0 \tag{A8}$$

$$\left.\frac{\partial y_2}{\partial \zeta_2}\right|_{\zeta_2=0} = -\mathrm{Pe} \cdot V_r(P_r \cdot y_1|_{\zeta_1=1} - y_2|_{\zeta_2=0})$$
$$\left.\frac{\partial y_2}{\partial \zeta_2}\right|_{\zeta_2=1} = 0 \tag{A9}$$

Step 2: blowdown step in bed 1 and pressurization step in bed 2

$$\left.\frac{\partial y_1}{\partial \zeta_1}\right|_{\zeta_1=0} = 0 \qquad \left.\frac{\partial y_1}{\partial \zeta_1}\right|_{\zeta_1=1} = 0 \tag{A10}$$

$$\left.\frac{\partial y_2}{\partial \zeta_2}\right|_{\zeta_2=0} = 0$$
$$\left.\frac{\partial y_2}{\partial \zeta_2}\right|_{\zeta_2=1} = \mathrm{Pe} \cdot V_2|_{\zeta_2=1}(y_f - y_2|_{\zeta_2=1}) \tag{A11}$$

Step 3: purge step in bed 1 and adsorption step in bed 2

$$\left.\frac{\partial y_1}{\partial \zeta_1}\right|_{\zeta_1=0} = 0$$
$$\left.\frac{\partial y_1}{\partial \zeta_1}\right|_{\zeta_1=1} = \mathrm{Pe} \cdot V_r(P_r \cdot y_2|_{\zeta_1=0} - y_1|_{\zeta_2=1}) \tag{A12}$$

$$\left.\frac{\partial y_2}{\partial \zeta_2}\right|_{\zeta_2=0} = 0 \left.\frac{\partial y_2}{\partial \zeta_2}\right|_{\zeta_2=1} = Pe(y_f - y_2|_{\zeta_2=1}) \tag{A13}$$

Step 4: pressurization step in bed 1 and blowdown step in bed 2

$$\left.\frac{\partial y_1}{\partial \zeta_1}\right|_{\zeta_1=0} = -Pe \cdot V_1|_{\zeta_1=0}(y_f - y_1|_{\zeta_1=0}) \tag{A14}$$

$$\left.\frac{\partial y_1}{\partial \zeta_1}\right|_{\zeta_1=1} = 0$$
$$\left.\frac{\partial y_2}{\partial \zeta_2}\right|_{\zeta_2=0} = 0 \qquad \left.\frac{\partial y_2}{\partial \zeta_2}\right|_{\zeta_2=1} = 0 \tag{A15}$$

The mole fractions at the surface and centre of the pellet are

$$y_p|_{\xi=1} = y \qquad \left.\frac{\partial y_p}{\partial \xi}\right|_{\xi=0} = 0 \qquad \text{(A16)}$$

During the steps in which the pressure varies with time, i.e. blowdown and pressurization, it is assumed that the pressure varies linearly with time over the entire step time from the pressure at the previous step to the pressure at the next step. For simplicity, the velocity is determined only by the change of pressure with time without considering the effect of adsorption and desorption. Therefore, the velocities are kept constant in adsorption and purge steps but it is changing in blowdown and pressurization steps:

$$\frac{dV}{d\zeta} = \frac{1}{W \cdot a \cdot \bar{P}} \frac{1 - P_r}{\tau_{BD}} \quad \text{for blowdown step} \qquad \text{(A17)}$$

$$\frac{dV}{d\zeta} = -\frac{1}{W \cdot a \cdot \bar{P}} \frac{1 - P_r}{\tau_{PR}} \quad \text{for pressurization step} \qquad \text{(A18)}$$

Nomenclature

a Dimensionless half cycle time (−)
c Concentration in the gas phase (mol/m^3)
c_{in} Inlet concentration (mol/m^3)
c_t Total concentration in the gas phase (mol/m^3)
C Dimensionless concentration (−)
D Diffusivity (m^2/s)
D_p Pore diffusivity (m^2/s)
D_{e} Effective diffusivity (m^2/s)
F Flow rate (m^3/s)
K Equilibrium constant, (−)
L Length of column (m) or Dimensionless parameter, Eq. (18) (−)
P Pressure (bar)
q Adsorbed amount (mol/m^3)
$\bar{q}$ Average adsorbed amount (mol/m^3)
Q Dimensionless adsorbed amount (−)
Pe Peclet number (−)
R_{b} Location of boundary in two-domain diffusion model (−)
R_p Radius of particle (mm)
t_{C} Half cycle time (s)
r Radial position in the particle (m)
v Interstitial velocity (m/s)
V_{s} Volume of solid phase (m^3)
V_{f} Volume of fluid phase (m^3)
W Dimensionless parameter, Eq. (A5) (−)
y Mole fraction (−)
z Axial position along the column (m)

Greek letters

ε Void fraction in the column, -
ε_p Particle void fraction (−)
γ Dimensionless parameter, Eq. (18) (−)
τ Dimensionless time (−)
τ_{AD} Dimensionless step time of adsorption step (−)
τ_{BD} Dimensionless step time of blowdown step (−)
τ_{PG} Dimensionless step time of purge step (−)
τ_{PR} Dimensionless step time of pressurization step (−)
ξ Dimensionless radial position (−)
ζ Dimensionless axial position (−)

Subscripts

1 Bed 1
2 Bed 2
H High pressure
i Inner domain of two-domain method
L Low pressure
o Outer domain of two-domain method
p Particle

Acknowledgments

Financial support from the Royal Society/Wolfson Research Merit Award and the Post-Doctoral Fellowship Program of the Korean Science & Engineering Foundation (KOSEF) is gratefully acknowledged.

References

Brandani, S. and D.M. Ruthven, "Analysis of ZLC Desorption Curves for Gaseous Systems," *Adsorption*, **2**, 133–143 (1996).
Crank, J., *The Mathematics of Diffusion*, 2nd edn., Oxford University Press, Oxford, 1975.
Nakao, S. and M. Suzuki, "Mass Transfer Coefficient in Cyclic Adsorption and Desorption," *J. Chem. Eng. Japan*, **16**, 114–119 (1983).
Nilchan, S. and C.C. Pantelides, "On the Optimisation of Periodic Adsorption Processes," *Adsorption*, **4**, 113–127, (1998).
Process Systems Enterprise LtD, gPROMS Advanced User Guide, London, 1999.

Raghavan, N.S., M.M. Hassan, and D.M. Ruthven, "Numerical Simulation of a PSA System Using a Pore Diffusion Model," *Chem. Eng. Sci.*, **41**, 2787–2793 (1986).

Rouse, A.J. and S. Brandani, "A New LDF Approximation for Cyclic Adsorption Processes," in P. Bryan and A. Serbezov (Eds.), *AIChE Separation Technology Topical Conference*, Vol. 2, pp. 739–743, 2001.

Stephanopoulos, G., *Chemical Process Control: An Introduction to Theory and Practice*. Prentice Hall, Englewood Cliffs, 1983.